Phase-shift mask technology: requirements for e-beam mask lithography

Steven K. Dunbrack, Andrew Muray, Charles Sauer, Richard L. Lozes
Etec Systems Inc., Hayward, California

John Nistler, William H. Arnold, David Kyser, Anna Minvielle, Moshe Preil,
Bhanwar Singh, Michael K. Templeton
Integrated Technology Division, Advanced Micro Devices, Sunnyvale, California

ABSTRACT

Phase-shifted patterns (alternating, 90-degree, and chromeless) have been incorporated into a reticle layout, fabricated with a MEBES® III system, and evaluated experimentally at 365 nanometers using steppers with numerical aperture (NA) ranging from 0.4 to 0.48 and partial coherence ranging from 0.38 to 0.62. Test circuit layouts simulate actual circuit designs with critical dimensions ranging from 0.2 μm to 1.2 μm. These results, combined with experimental measurement of layer to layer registration and aerial image simulations, provide a first-order assessment of e-beam lithography requirements to support phase-shift mask technology.

1. INTRODUCTION

The application of optical phase shifting for improving resolution, image intensity, and depth of focus is a technique[1] whose advantages have recently been recognized in optical microlithography[2]. Compared to changing the wavelengh or numerical aperture of a reduction stepper, the incorporation of phase-shifters onto a reticle is a desirable alternative for improving resolution and/or depth of focus at an acceptable image intensity. Although the principles of optical imaging and phase shifting are well understood, the methodology for designing a phase-shift pattern and converting it into an image on the wafer involves many tradeoffs and several alternative approaches[2-5]. The classification of phase-shift pattern types here follows the conventions used in reference 5.

To characterize the tradeoffs associated with the fabrication of recticles with phase-shift patterns, an investigation was undertaken whose purpose was twofold: (1) demonstration of a phase-shift mask technology with designs that can readily be applied to the next generation of devices, and (2) evaluation of e-beam tool requirements for supporting phase-shift mask technology from these experimental results and simulations.

2. PHASE-SHIFT MASK TECHNOLOGY TEST VEHICLE

Reticles incorporating phase-shift designs have been fabricated using the procedure shown in Figure 1a. Masks were prepared in two separate steps. The first layer was prepared by writing on vendor-coated 4000Å PBS resist spun on five-inch chrome-coated quartz blanks. The exposure dosage used for this layer was 1.0 $\mu C/cm^2$. The resist was developed using standard PBS spray development techniques. After development, the chrome was wet-etched using Cyantek™ CR-14, and the resist was stripped.

A second layer was prepared by treating the mask with HMDS, coating it with 3600Å of PMMA, and evaporating a thin (~150Å) layer of aluminum. The aluminum is used as a charge-dissipation layer. The second layer was written with an exposure dose of 120 $\mu C/cm^2$. Prior to writing the mask, the direct-write option of the MEBES system was used to locate three flag marks written on the first layer of the mask. The placement of the second layer was adjusted to correspond to the locations of the flag marks written on the first layer.

Both layers were written on a MEBES III system at 10 KeV, typically with an address of 0.25 μm. After exposure, the mask was treated briefly with a dilute caustic solution to remove the aluminum, and the PMMA was developed. Development was done in a spray developer. After a post exposure bake, the plate was ready for inspection and use as a phase-shift mask.

 0-8194-0563-9/91/$4.00

The test circuits for lithography evaluation are modified Prometrix-style defect density test chips containing four modules ranging from 0.2 μm features up to 1.2 μm line/space pairs. A module used as the statistical control contains only normal mask layout designs in chrome. Other modules use a layout similar to the first but with phase-shifting elements of various design for evaluation. All structures can be examined by SEM or by electrical testing. Figure 1b shows an example of a device area on the fabricated reticle. The bright regions in the micrograph correspond to the overlap region between PMMA and chrome.

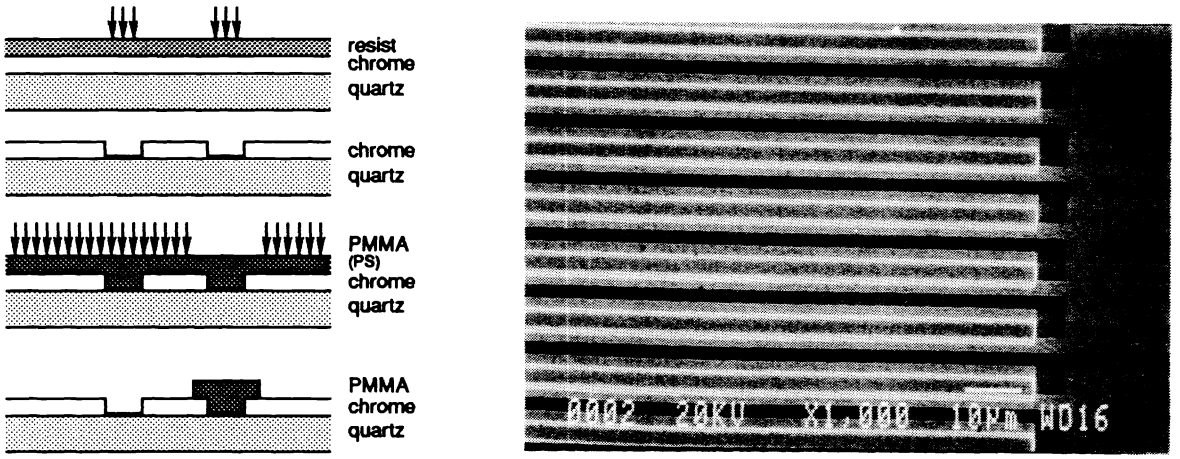

Figure 1. (a) Phase-shifted mask cross-section diagram (b) SEM micrograph of phase-shifted mask structure.

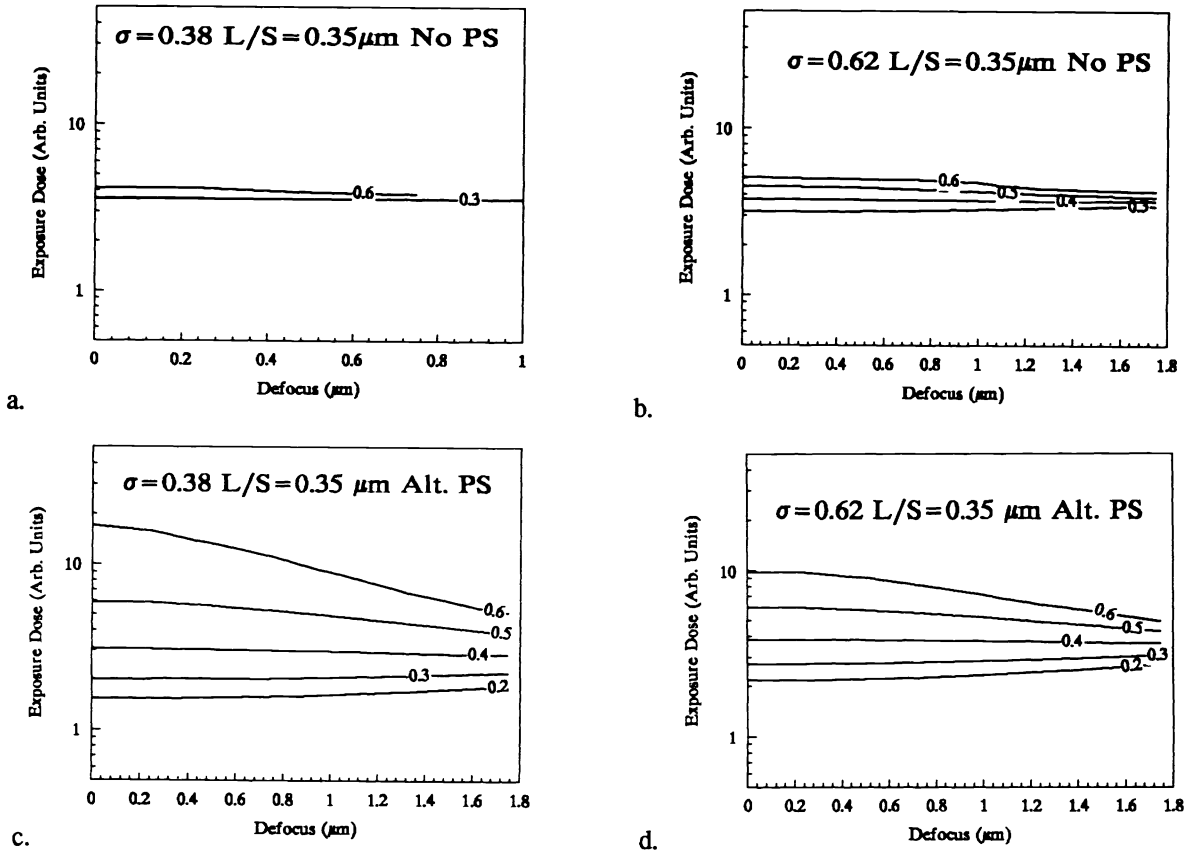

Figure 2. Exposure defocus diagrams for alternating phase modulation versus normal grating patterns for partial coherence of 0.38 and 0.62.

3. OPTICAL LITHOGRAPHY SIMULATIONS AND EXPERIMENTS

3.1 Optical lithography modeling

In the design and characterization of phase-shift patterns, simulation is helpful in visualizing and verifying results. SPLAT, based on the Hopkins model of partial coherence[6], was used to calculate aerial images resulting from phase-shift patterns. Equi-energy contours represent lithography patterns. To characterize the behavior of patterns in exposure-dose space and to evaluate the proximity effect, exposure-defocus (ED) diagrams[7] derived from aerial images were generated and used to compare the responses of various patterns.

3.2 Alternating phase-shift gratings

One of the first experimental investigations was the comparison of non-phase-shifted grating structures and and alternating phase-shifted gratings. As shown by Levenson *et al.*[2], reduction in the partial coherence improves contrast for both shifted and unshifted structures. For totally incoherent illumination, the contrast curves of both patterns become indistinguishable. Figure 2 shows exposure-defocus diagrams derived from simulations for 0.3 μm line/space (0.38 λ/NA) using partial coherence of 0.38 and 0.62 (NA=0.4, λ=0.365). These results indicate an improvement in depth of focus with phase-shifting, which is more significant for lower partial coherence.

Figure 3 illustrates the difference between phase-shifted and unshifted patterns (consistent with the simulations). A 0.35-μm line/space pattern was overexposed to print a 0.2/0.5 μm serpentine pattern using alternating phase-shifting. Note that the unshifted pattern has not cleared and that the image is starting to deteriorate. The results are from the same field of exposure on the same wafer. The stepper used was an ASML 5000/50, NA of 0.48, partial coherence of 0.62. The resist used was Shipley 3813, thickness of 1.01 μm, single wafer immersion with a 115°C postexposure bake. Further comparisons between simulated aerial image contours and experimental results are shown in Figure 4 (unshifted) and Figure 5 (shifted) for 0.9 and 1.5 μm of defocus (NA=0.4, sigma=0.54). Note that the change in linewidth as a function of defocus is less for the phase-shifted pattern in the x direction, but not in the y direction.

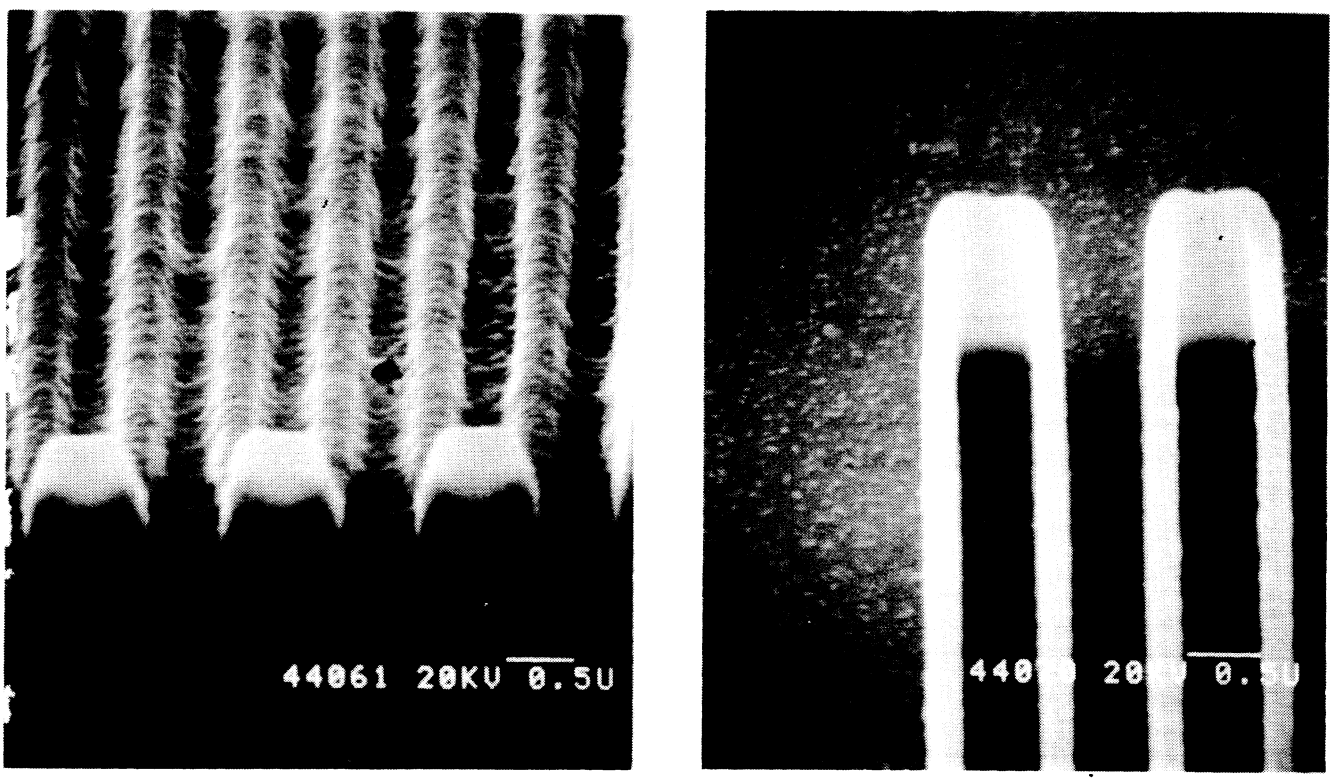

Figure 3. Experimental comparison of normal and PMMA-generated alternating phase-shifting reticle: 0.35 line/space. (a) Normal serpentine pattern. (b) Alternating grating structures exposed at 0.3 μm defocus at 170 mj. Resist type is Shipley 3813, 115° PEB.

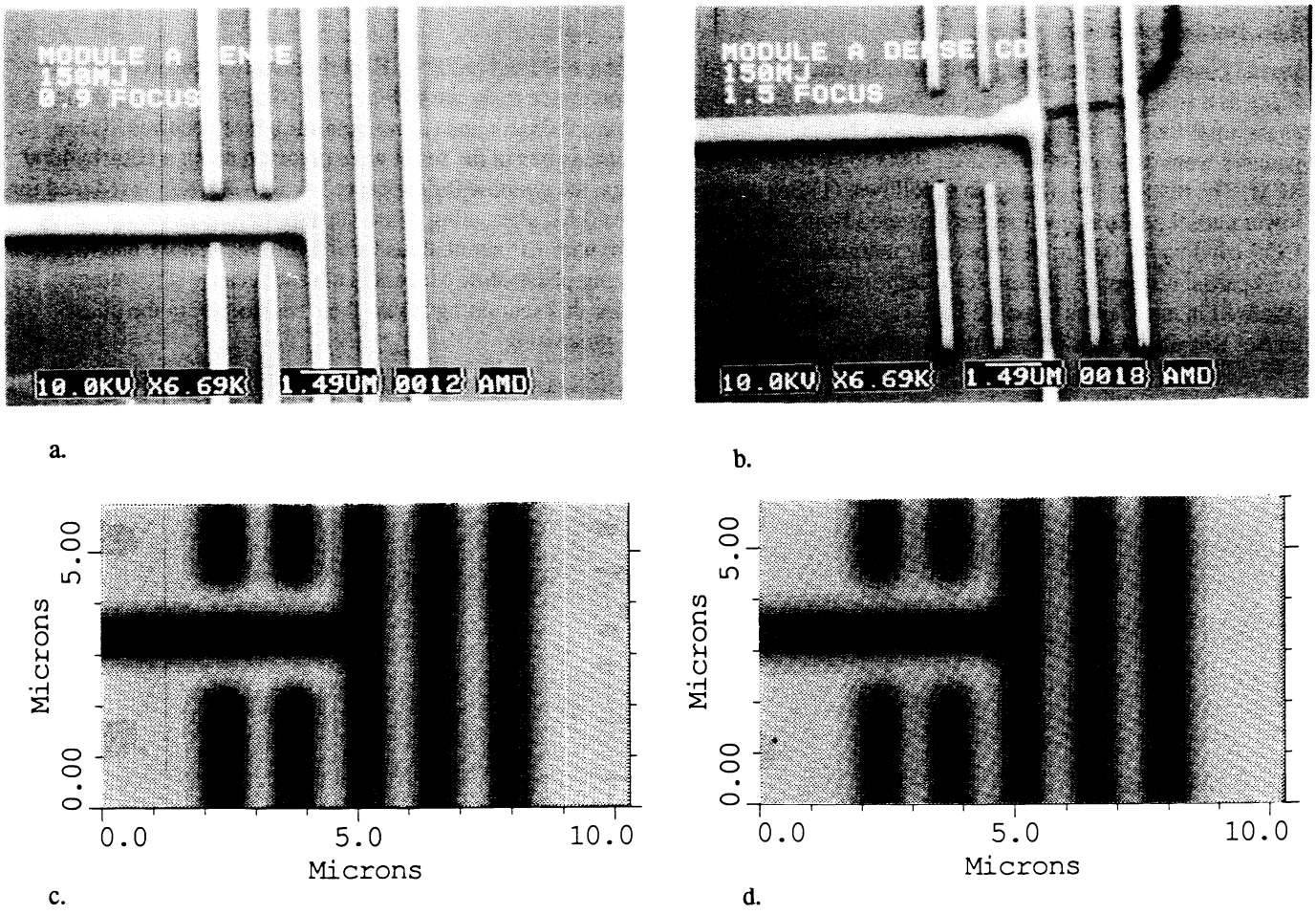

Figure 4. SEM micrographs of test structure at (a) 0.9 and (b) 1.5 μm defocus compared to simulation results (c, d) with no phase shifting.

3.3 0/90/180 degree phase-shift results

In an effort to overcome the limitation of the zero node between the 0/180 phase transition visible in the serpentine pattern (Figure 5), designs incorporating 0/90/180 phase shifters were attempted[11]. From aerial image simulations (Figure 6a), it is found that the null in the transition can be avoided if a 90° phase-shift region is used, as shown in the pattern. A reticle with this pattern has been fabricated and is shown in Figure 6b. Ninety-degree phase-shift regions are formed by double exposure during the phase-shift exposure (with no additional overlay), and is apparent in the micrograph from the narrower linewidth. Optical lithography was carried out in an I-line GCA stepper with 0.45 NA and a partial coherence of 0.58. Micrographs of resist on silicon after exposure at defocus values of 0.2 and 0.6 μm are shown in Figure 6c and 6d. At 0.2 μm defocus, the 0/90/180 transition region has cleared, but at 0.6 μm bridging is observed. A qualitative comparison between the simulation and experimental results suggests that pattern distortion and bridging occur as a result of lower intensity in the transition region.

3.4 Chromeless phase-shift results

A chromeless phase-shifted pattern was formed by a 180 to 0 phase-shift edge as demonstrated in Figure 7a. The 0.7-μm line/space next to the chromeless feature were used to set focus and exposure conditions. Figure 7b shows the chromeless phase-shifting structures after exposure in an ASML PAS 2500/40 stepper. The NA was 0.40 and partial coherence was 0.54. The resist used was Shipley 3813 (I-line positive resist) using a spray-puddle develop process. The resist aspect ratio is 6 to 1. The developed feature is slightly smaller than nominal as a result of overdevelopment. (Note: Metrology for 0.7-μm line/space patterns is well characterized. Further work remains to determine accurate measurement techniques for linewidths of 0.2-μm dimension[8].)

3.5 Partial coherence effects

Partial coherence effects were compared for normal and alternate phase-shifted patterns. Experimentally measured depth of focus as a function of exposure dose for various values of partial coherence is shown in Figure 8a. Depth of focus is defined as the total focus window inside of which (1) the linewidth is 0.5 μm ±0.05 μm and (2) no scumming has occurred. These patterns were exposed in an ASML 5000/50 stepper, and critical dimensions in the resist were obtained using a Hitachi 4000 SEM. The results of this data are as follows. (1) For normal gratings, the window for exposure for a given DOF is reduced for lower partial coherence values, as expected from simulations. (2) At 0.62, alternating phase shifting improves the operating DOF window for 0.5 μm features only marginally (again, consistent with ED simulations for 0.5 μm line/space), and (3) at 0.38 partial coherence, the expected improvement by using alternating phase-shift patterns is absent because scumming occurred in every other exposed line. The most likely explanation for this scumming is that the transmission in the phase-shifter was different from that in the unshifted region as a result of processing.

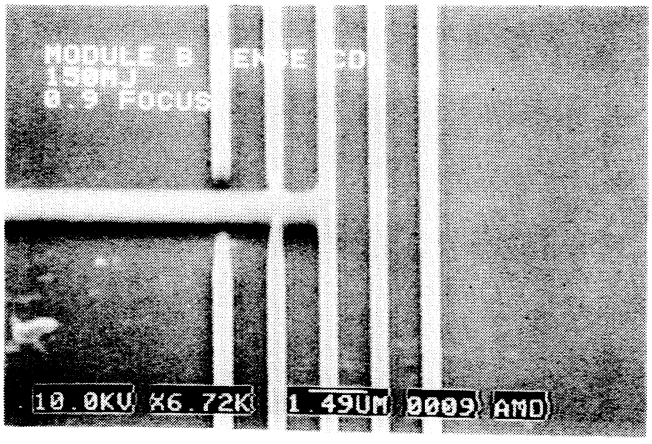

a.

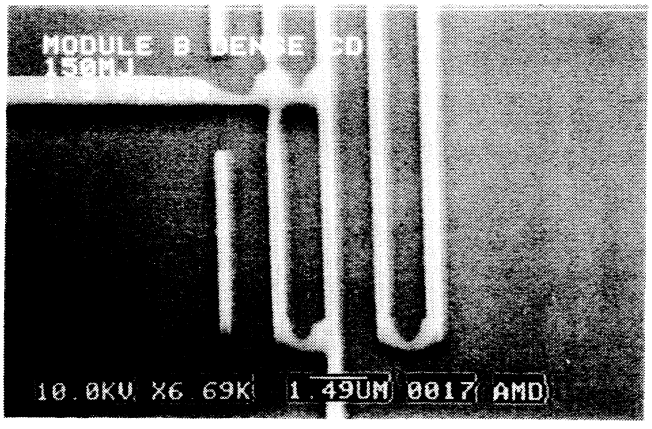

b.

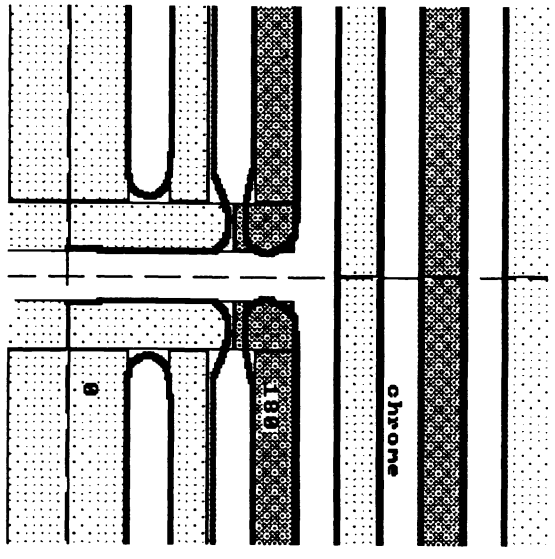

c.

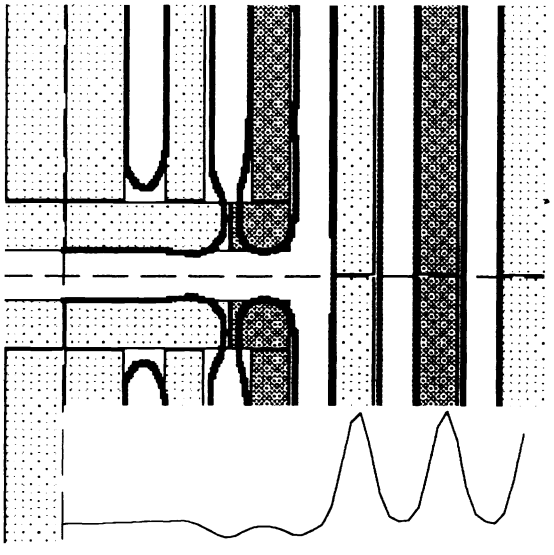

d.

Figure 5. SEM micrographs of test structure at (a) 0.9 and (b) 1.5 μm defocus compared to (c, d) simulation results for phase-shifted results. Inset in Figure d shows aerial image profile along the symmetry axis indicated in c.

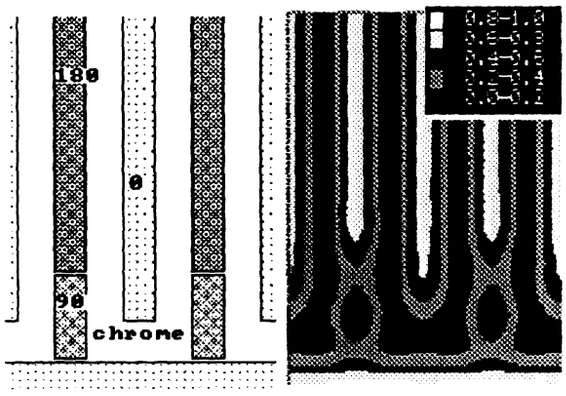

a.

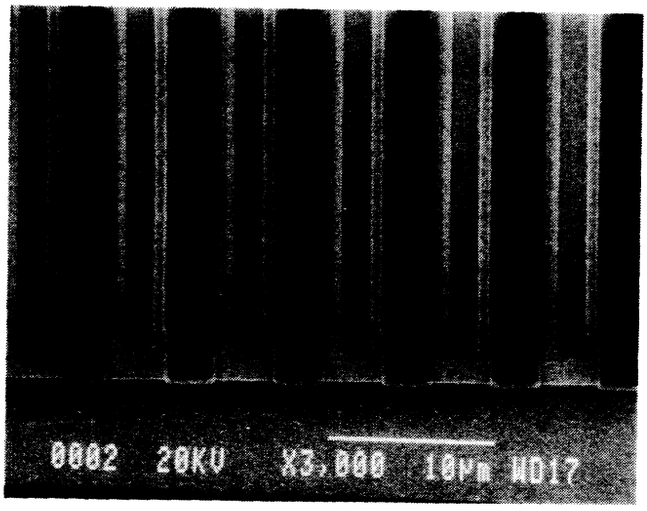

b.

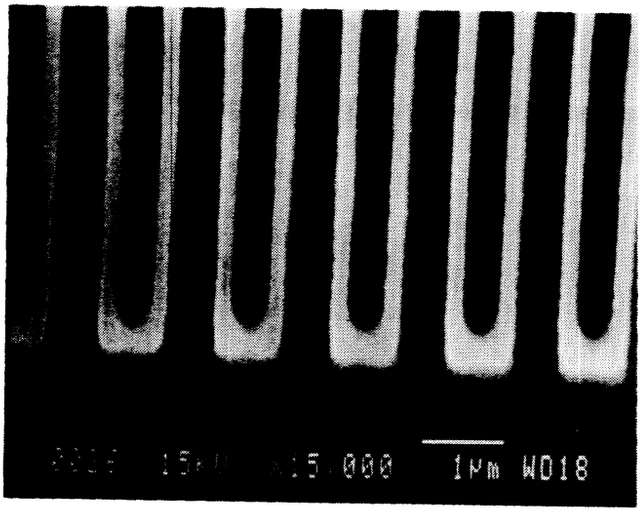

c.

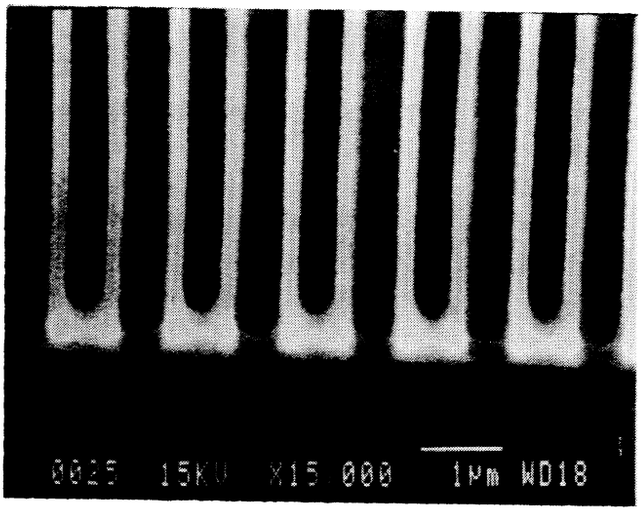

d.

Figure 6. (a) Simulation of 0/90/180 phase-shift serpentine pattern. Wavelength=365 nm, defocus=0.2 µm, NA=0.45, σ=0.58. (b) Reticle fabricated using pattern in a. (c) Optical results: resist on silicon at 0.2 µm defocus for above reticle. (d) Same as c at 0.6 µm defocus.

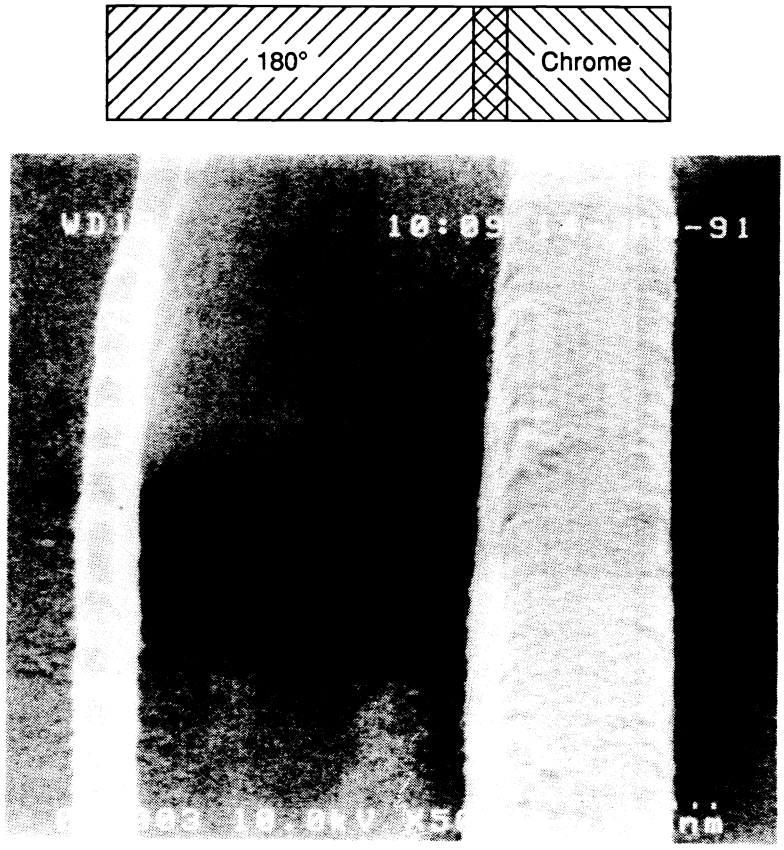

Figure 7. Chromeless phase pattern: isolated resist line. Top diagram indicates the original pattern.

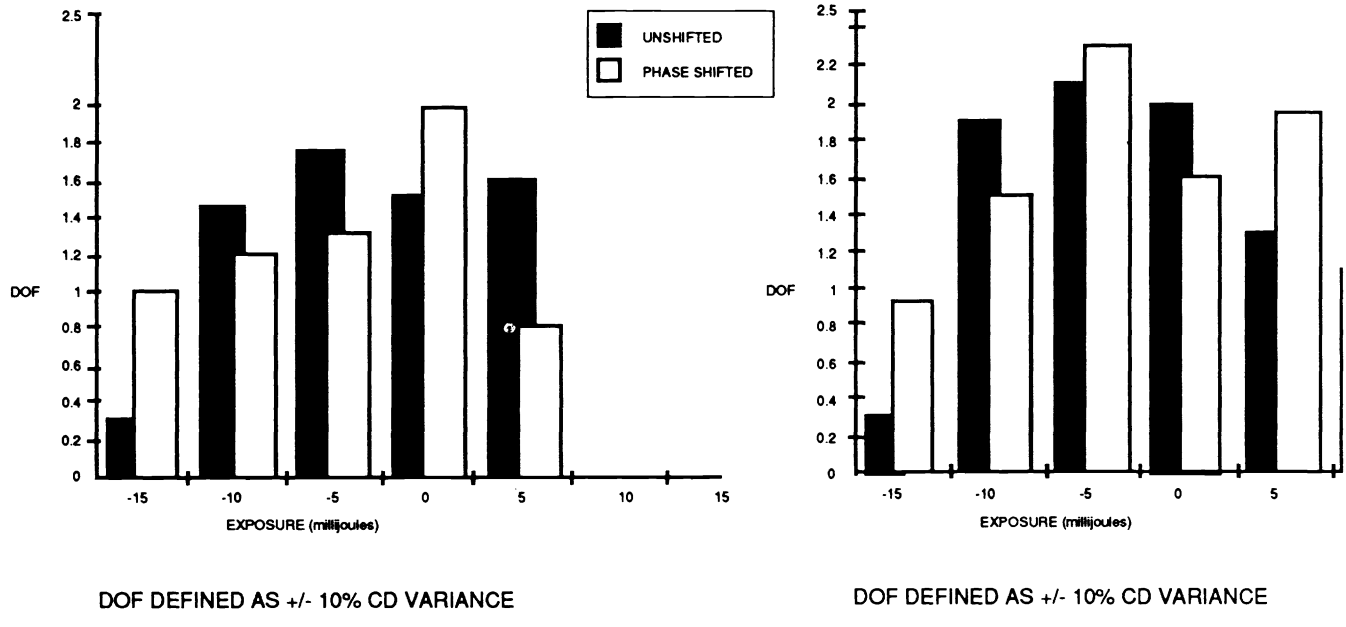

Figure 8. Partial coherence effects: comparison of depth of focus versus exposure dose at 0.38 + 0.62 partial coherence for phase and normal grating patterns.

4. RETICLE FABRICATION SENSITIVITIES

Requirements for phase-shift mask fabrication were determined from a sensitivity analysis of the various phase-shift mask techniques to e-beam lithography parameters. These parameters include overlay, critical dimension (CD) uniformity, resolution, corner rounding, phase error (thickness variation), and mean-to-nominal linewidth deviation. Some phase-shift techniques are more sensitive to a particular parameter than others and, therefore, some are not considered. A table at the end of this section summarizes the results.

4.1 Overlay

Two separate tests were made to verify overlay. A PBS/PMMA mask was prepared according to the procedure outlined above. The data for this mask contained a vernier pattern. A second test was made using a PBS/PBS mask with a nine-by-nine series of crosses. After processing both layers, the plate was recoated with aluminum and the overlay measured on both MEBES and AEBLE™ systems. Figure 9 is a histogram generated on AEBLE, which shows that the overlay between the two layers is essentially zero.

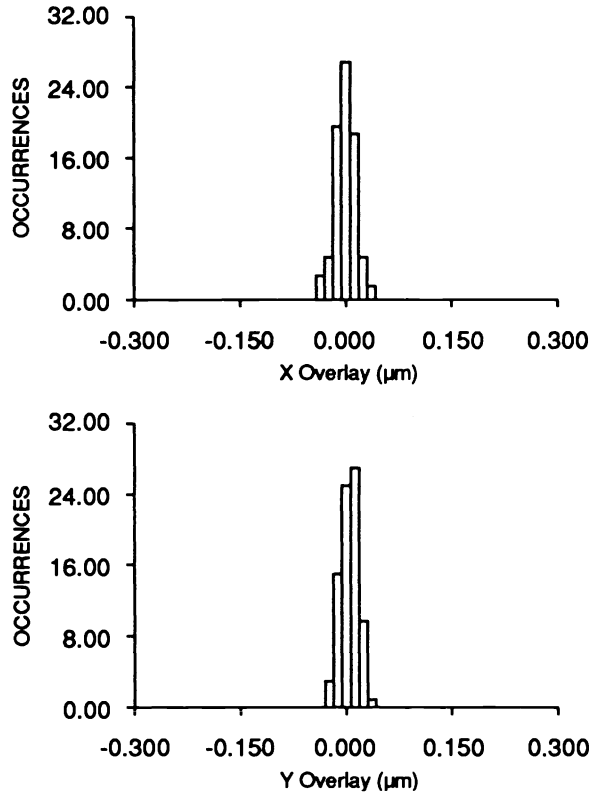

Die Index 3	X	Y
Mean	-0.0071	-0.0020
Max	0.0310	0.0310
Min	-0.0480	-0.0310
Sigma	0.0151	0.0132
Mean+3.0 sig	0.0523	0.0417
% < 0.150:	100.00	100.00
Measurement Err.	0.0032	0.0043
With Repeatability Correction:		
Sigma	0.0147	0.0125
Mean+3.0 sigma	0.0513	0.0395

Figure 9. Measurement of overlay error on a MEBES III system.

Although the structures fabricated for this study are not particularly sensitive to misalignment, simulations on phase-shifted contacts (Figure 10a) show that misalignment (assuming the auxiliary features are patterned in the second exposure) of 0.1(x5) μm results in 0.05 μm shift in the printed contact. A pattern misplacement of 0.1 μm in the auxiliary shifters on the reticle, for example, would result in shift of 0.01 μm in the printed contact.

4.2 Critical dimension uniformity

Simulations on auxiliary and alternating phase structures show minimal increase in CD sensitivity over normal structures, except for chromeless phase-shift type patterns, which show a significiant increase. An example (Figure 10b), where the chrome has been replaced with a dark field grating and the linewidth has been perturbed by 0.1 μm, shows a large response at both 0.0 and 2.0 μm defocus. The sensitivity to the CD change in the chromeless case increases by approximately a factor of 4 over the normal line (365 nm, NA=0.4, pc=0.54, nominal linewidth=0.4 μm).

4.3 Mean linewidth deviation and phase error

Figure 10d shows the image intensity resulting from perturbations on the dark field line dimension and the phase change in the pattern area, illustrated in Figure 10c. These simulations indicate that for dark field structures, the 180° line CD is critical to determining dark region intensity. As a reference point, 800Å of chrome typically reduces light intensity by a factor of 0.1% in background intensity, whereas a 10% change in linewidth in the dark field pattern results in a 1% increase in background illumination. Overall phase error (thickness variation) can also contribute to dark area illumination as shown in case e of Figure 10d.

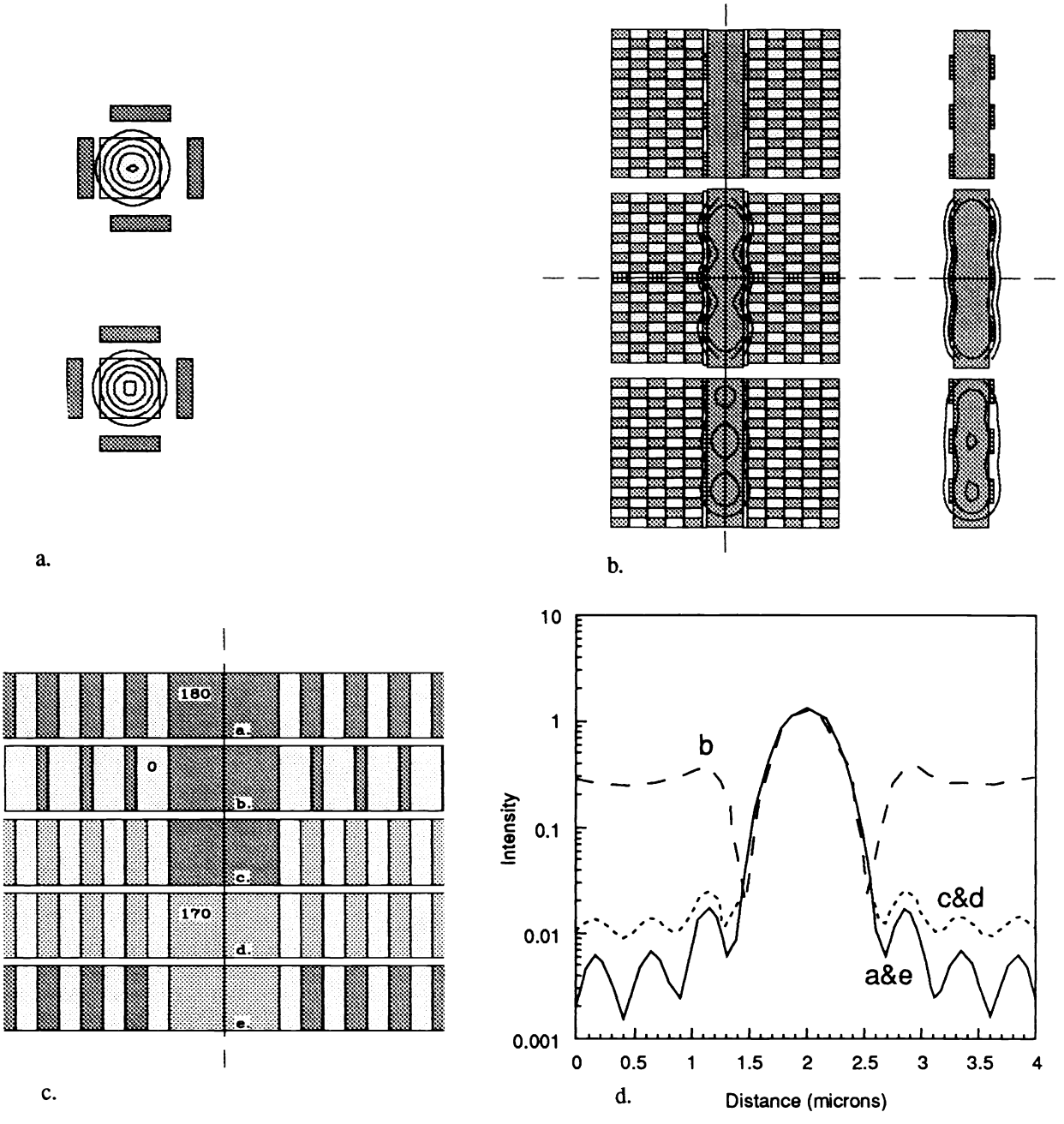

Figure 10. (a) Auxiliary-type phase-shift structure sensitivity to misalignment of phase shifters: 0.1 μm misalignment on mask results in 0.01 μm on wafer. (b) Comparison of aerial image intensity contours of chromeless/normal isolated lines after CD perturbation. (c) Patterns used in mean linewidth and phase error simulation. (d) Intensity profiles as a function of dark field grating linewidth.

4.4 Resolution

The minimum feature sizes found in phase-shift patterns are typically the outriggers in the auxiliary-type contacts and dark field gratings in the chromeless-type phase-shift patterns. The dimension of these patterns is 0.2 x λ/NA, which is much smaller than for conventional masks. As an example, a contact with auxiliary structures may require the structures to be 0.55 μm = 5 x (0.15 x 0.365 nm/0.5). An example of a contact with the auxiliary structures after primary exposure on the recticle is shown in Figure 11a, written using GHOST™ proximity correction[9] with 0.1 μm spot size and address unit size. Dark field grating structures in the chromeless-type phase-shift patterns also require minimum features in the submicron range.

Another observation for chromeless-type patterns is that resolution of dark field structures in the chromeless type of phase-shifter influences the deviation from nominal as indicated in Figure 11b.

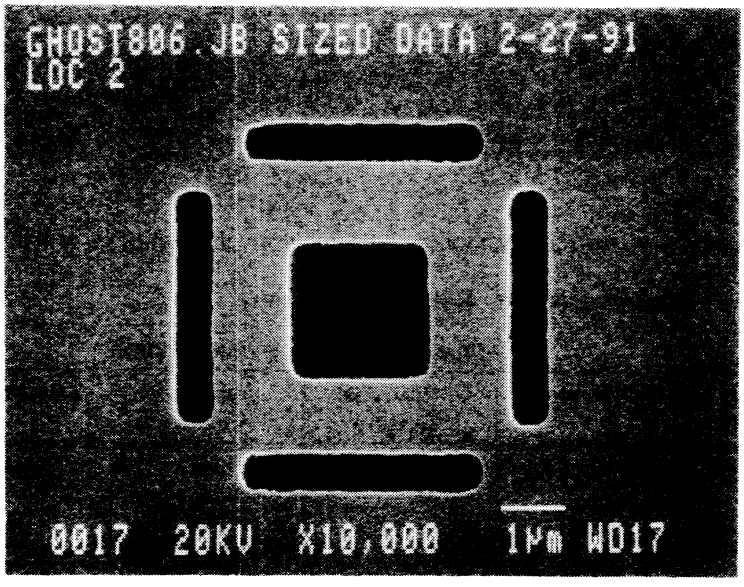

a.

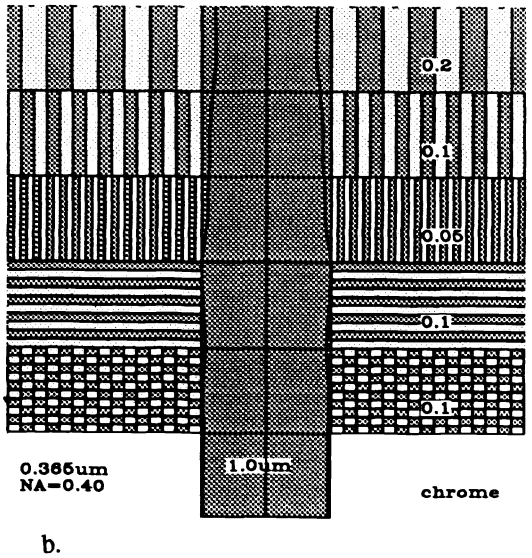

b.

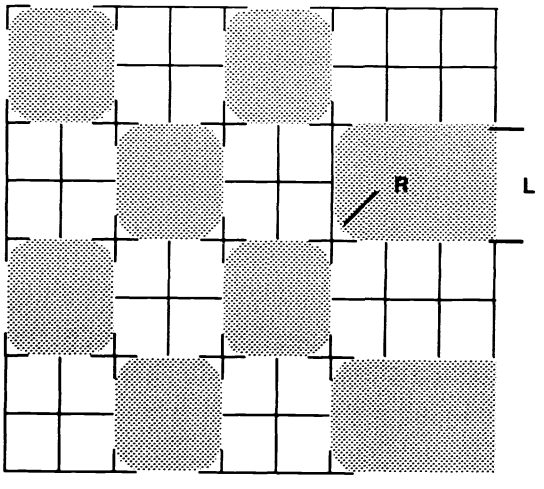

c.

Figure 11. Chromeless phase-shift structures. (a) SEM micrograph of auxiliary-type 0.4 μm contact with 0.1 μm outriggers after primary exposure and chrome etching. (b) Effect of dark field pattern orientation and linewidth on wafer CD. (c) Diagram defining residual area in dark field pattern.

4.5 Corner rounding

In addition to resolution, corner rounding of the minimum features is a significant factor because differences in total phase-shifted area to unshifted area result in illumination in the dark regions. (Assuming both checkboard and line grating are used, it is not possible to bias the data to avoid leakage in both areas simultaneously.) Let the residual area be the difference in nominal pattern area to actual phase-shifted area (Figure 11c). Residual area as a function of R/L can be calculated and is also shown below.

Corner Rounding Effects in Dark Field Patterns
Residual area (phase shifted–unshifted area) as a function of R/L

R=Radius of beam **L=Design length of pattern**

R/L	Residual Area (LxL=1)
0.5	21.4%
0.25	5.36%
0.125	1.34%

4.6 Summary of sensitivities

The following table summarizes phase-shift technology sensitivities to electron-beam reticle fabrication parameters.

Requirements for E-Beam Lithography

	Phase-Shift Mask Structure Type			
E-Beam Parameter	**Self-Aligned**	**Alternate Grating**	**Assistant Feature**	**Chromeless**
Charge dissipation	no	yes	no	yes
Alignment	no	yes	yes	no
Resolution	1 μm	1.0 μm (0.5 μm subphase)	0.5 μm	0.5 μm (maybe 0.25 μm)
CD control	0.05 μm	not critical	0.05 μm	0.0125 μm
Registration	n/a	not critical	0.1 μm	butting 0.05 μm
Corner rounding	n/a	not critical	0.25 μm	0.1 μm
Second exposure	no	yes	yes	no

Note: All dimensions measured on mask.

5. DISCUSSION

The use of a charge dissipation layer is crucial to the patterning of a phase-shift mask using electron beam lithography at 10 KeV. Several attempts were made to forego this step. Pattern distortion and misalignment resulted from charging of the mask. The degree to which this phenomenon takes place depends largely on the amount of chrome remaining on the first layer. The majority of materials suggested as phase-shifters will act as insulators. Preferable to the current technique would be the use of a conductive resist, use of a conductive phase-shifter material, or the adaptation of a conductive layer that is easy to apply and remove.

Mark finding proved to be an easy task with these materials; however, one problem was encountered. Mark finding with PMMA sandwiched between chrome and aluminum causes the resist to bubble and bake on the flags. This phenomenon is caused by the electron beam heating the resist. Locating the marks a second time, even with no intervening processing, proved to be difficult with this material. Aggressive cleaning techniques must be developed if using marks over is desired. It would be desirable to reclaim a mask when a mistake has been made on the second layer that occurred prior to etching.

One interesting observation from this study is that the use of phase-enhanced reticle coating (PERC) improves the relative depth of focus associated with line/space pairs (Figure 12). Some simulation results will be shown in another paper at this conference[10]. The patterns shown were exposed in an ASML PAS 2500/10, G-line stepper with an NA of 0.38 and partial coherence of 0.58. Results have also been obtained at I-line at 0.4 μm and are similar to the G-line results.

Design of practical structures was one of the goals of this study. Although some useful devices can be made using 180 phase-shifters, an obvious limitation is in the connection of a 180 phase-shifted line to an unshifted region. One solution is to use a 90-degree shifter, as shown in above. A limitation of this approach using the above design is the loss in the depth of focus and distortion in the transition region. Further improvement has been found by using 0/60/120/180 shifters in the transition region, as shown in Figure 13.

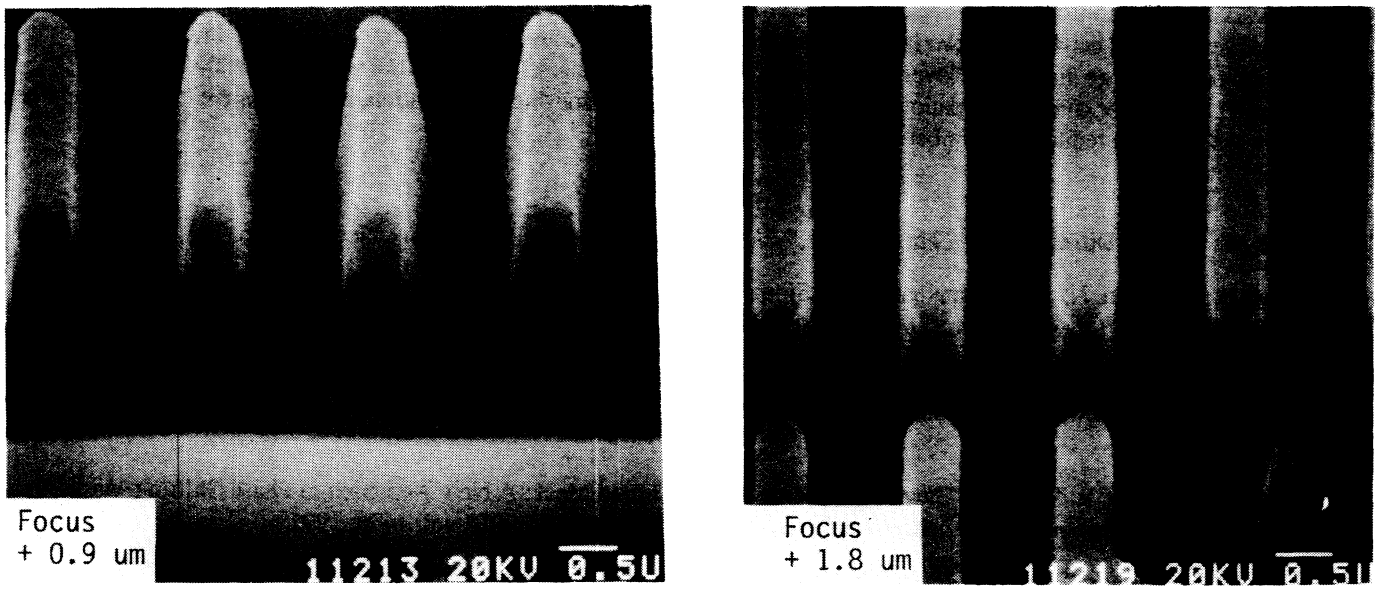

Figure 12. Phase-enhanced reticle coating (PERC) 0.5 μm line/space exposed in ASM PAS 2500/10 G-line stepper, NA=0.38, PC=0.58. Note improvement at 1.8 μm defocus with PERC compared to 0.9 μm defocus with no PERC.

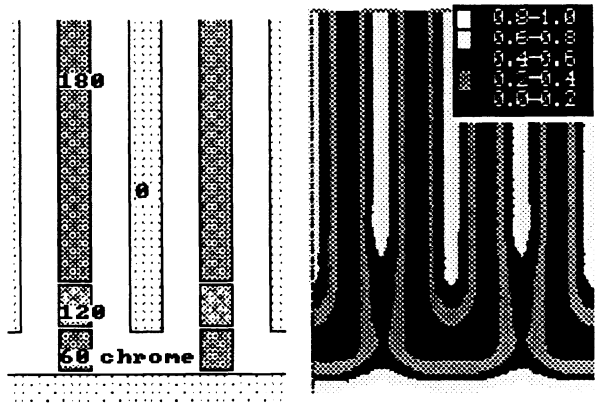

Figure 13. Simulation of 0/60/120/180 phase-shift serpentine pattern.

6. CONCLUSION

Investigation of alternating phase-shift patterns has confirmed that experimental resolution and depth of focus agree with simulation results. ED diagrams (Figure 2) indicate that for unshifted patterns, the process window is smaller than for phase-shifted patterns. This is consistent with the measurements of depth of focus at partial coherence values of 0.62 for both 0.35 and 0.5 μm line/space features. Experimental measurement of DOF for phase-shifted gratings at 0.38 partial coherence disagreed with simulation results for these patterns. Scumming in the phase-shifted lines was observed and points to the possibility of transmission mismatch between phase-shifted and unshifted areas. Experimental verification of 90° phase-shifter effects has led to further development of practical design layouts, and chromeless phase-shift patterns have also been made with 0.2 μm dimensions.

Fabrication of the reticles and sensitivity analysis of phase-shift patterns have led to a first order analysis of requirements for e-beam fabrication of various phase-shift technologies. It was found, for example, that mean-to-nominal linewidth deviation, thickness variation, CD uniformity, and resolution are critical for chromeless phase-shift patterns using dark field grating structures. Overlay error between the two layers (if needed) depends on the amount of coverage of the two layers and the effectiveness of the charge dissipation layer. Simulations show that tolerances for overlay are within current MEBES capabilities (0.1 μm). For charge dissipation, aluminum was satisfactory for this investigation, but alternative means should be explored in the future to reduce the number of processing steps.

7. REFERENCES

1. R. W. Wood, "Diffraction by Thin Laminae," *Physical Optics*, Dover Publications, New York, p. 201, 1905.

2. M. D. Levenson, N. S. Viswanathan, R. A. Simpson, "Improving Resolution in Photolithography with a Phase-Shifting Mask," *IEEE Trans on Electron Devices*, vol. Ed-29, No. 12, pp. 1812–1846, Dec. 1982.

3. A. Nitayama, T. Sato, K. Hashimoto, F. Shigemitsu, N. Nakase, "New Phase-Shifting Mask with Self-Aligned Phase-Shifters for Quarter Micron Photolithography," *Proceedings of SPIE: Optical/Laser Microlithography*, vol. 1088, pp. 25–33, 1989.

4. K. Toh, G. Dao, R. Singh, H. Gaw, "Chromeless Phase-Shifted Mask: A New Approach to Phase-Shifting Masks," *Proceedings of the Tenth Annual Symposium on Microlithography, Sept. 1990*, SPIE vol. 1496, 1991.

5. A. R. Neureuther, "Modeling Phase Shifting Masks," *Proceedings of the Tenth Annual Symposium on Microlithography*, SPIE vol. 1496, 1991.

6. P. D. Flanner III, S. Subramanian, A. R. Neureuther, "Two-Dimensional Optical Proximity Effects," *Optical Microlithography V*, SPIE vol. 633, 1986, pp. 239–244.

7. B. Lin, "Phase-Shifting and Other Challenges in Optical Mask Technology," *Proceedings of the Tenth Annual Symposium on Microlithography, Sept. 1990*, SPIE vol. 1496, 1991.

8. K. Phan, J. Nistler, B. Singh, "Metrology Issues for Submicron Lithography," *Proceedings of SPIE*, vol. 1469, 1991.

9. A. Muray, R. L. Lozes, K. Milner, G. Hughes, "Proximity effect correction at 10 KeV using GHOST and sizing for 0.4 micron mask lithography," *J. Vac. Sci. Technol.* **B**. vol. 8, No. 6, Nov/Dec 1990, pp.1775–1779.

10. T. Doi, K. M. Tadros, A. R. Neureuther, V. Kuyel, "Edge-Profile, Materials, and Protective Coating Effects on Image Quality," *Proceedings of SPIE*, vol. 1464, 1991.

11. J. Miyazaki, K. Kamon, N. Yoshioka, S. Matsuda, M. Fujinaga, Y. Watakabe, and H. Nagata, "A New Phase Shifting Mask Structure for Positive Resist Process," *Proceedings of SPIE*, vol. 1464, 1991.